IEEE Access
Multidisciplinary ⋮ Rapid Review ⋮ Open Access Journal

Received 17 May 2022, accepted 21 June 2022, date of publication 29 June 2022, date of current version 8 July 2022.

Digital Object Identifier 10.1109/ACCESS.2022.3187003

RESEARCH ARTICLE

Nonlinear Positioning Technique via Dynamic Current Cut-Off Frequency and Observer-Based Pole-Zero Cancellation Approaches for MAGLEV Applications

SUNG HYUN YOU[1], KI-CHAN KIM[2], (Member, IEEE), HYUN HO KANG[3], KWAN SOO KIM[3], AND SEOK-KYOON KIM[4]

[1]Department of Electronic Engineering, Chosun University, Gwangju 61452, South Korea
[2]Department of Electrical Engineering, Hanbat National University, Daejeon 34158, South Korea
[3]School of Electrical Engineering, Korea University, Seoul 136701, South Korea
[4]Department of Creative Convergence Engineering, Hanbat National University, Daejeon 34158, South Korea

Corresponding author: Seok-Kyoon Kim (lotus45kr@gmail.com)

This work was supported in part by the Basic Science Research Program through the National Research Foundation of Korea (NRF) by the Ministry of Education under Grant 2018R1A6A1A03026005, in part by the National Research Foundation of Korea (NRF) by the Korean Government through the Ministry of Science and ICT under Grant NRF-2021R1C1C1004380 and Grant NRF-2020R1G1A1103036, and in part by the National Research Foundation of Korea (NRF) funded by the Korea Government (MSIT) under Grant 2020M3H4A3106326.

ABSTRACT This article solves the problem caused by high level current feedback gain setting for fast responsiveness of magnetic levitation systems considering the current dynamics and presents advanced nonlinear positioning technology without plant parameter information. The main features of this study are summarized as follows: First, current control demonstrates current ripple reduction and overall performance guarantee through a low feedback gain in the steady state, including a dynamic feedback loop increased by an error variable magnitude in the transient period. Second, the plant parameter information-free velocity observer replaces the observer output error integral action with the disturbance estimation action to improve the closed-loop performance. The simulation results reveal the practical advantages derived from the contributions of this study.

INDEX TERMS Magnetic levitation, positioning, variable cut-off frequency, velocity observer, disturbance observer.

NOMENCLATURE

PLANT VARIABLES

M, M_L	Masses of electromagnet and load.
g, K	Gravitational acceleration and electromagnetic force coefficient.
R_c, L_c	Coil resistance and inductance.
$M_0, K_0, R_{c,0}, L_{c,0}$	Norminal parameter values.
$\bar{w}_p, \bar{w}_c$	The uncertain time varying disturbances.
p, v_p, i_c, V	Position, velocity, current, voltage of MAGLEV system.
p^*, i_c^*	Desired position and coil current.
$p_{ref}, i_{c,ref}$	Reference position and coil current.
ω_c, ω_p	Cut-off frequencies.

CONTROLLER VARIABLES

e_p, e_v	Estimation errors of position and velocity.
$d_p, \hat{d}_p, d_c, \hat{d}_c$	Lumped disturbance and disturbance estimation.
$l_{v,i}$	Design parameters of velocity observer.
z_{ref}	Control input variable.
$\tilde{p}$	$p_{ref} - p$ error.

The associate editor coordinating the review of this manuscript and approving it for publication was Philip Pong.

$b_{d,p}$, l_{d_p}	Observer-based DOB gains in outer loop.
Δi_c^*, Δi_c	$i_{c,ref} - i_c^*$ and $i_c^* - i_c$ errors.
$\hat{\omega}_c$	Boosted cut-off frequency.
κ_{ω_c}, ς_{ω_c}	Dynamic feedback loop gains.
$b_{d,c}$, l_{d_c}	Observer-based DOB gains in inner loop.

I. INTRODUCTION

Mass positioning tasks can be accomplished by the electromagnetic force caused by the coil current, which paly a vital role in magnetic levitation (MAGLEV) technique-based industrial trains. MAGLEV trains have been considered an alternative to conventional engine-based systems because of their decreased pollution and noise levels and increased durability [1]–[5].

The current and position dynamics are coupled with a nonlinear relationship in the presence of mismatched disturbances by the sudden increase/decrease in the number of passengers, which makes it nontrivial to solve the positioning problem of MAGLEV systems [6]–[8]. Moreover, variations in the coil inductance and resistance value are also problematic, leading to inconsistent closed-loop performance over a wide operating region. The linearization technique can transform nonlinear dynamics into an unstable linear system with limited admissibility, which helps in solving the positioning problem using a simple proportional-integral (PI) controller [9]. State-feedback control with feed-forward compensation terms has been presented as another linearization-based solution with improved closed-loop performance assignability via the pole placement technique [9], [10]. The resultant closed-loop performance obtained from these linear controllers can be limited when considering the feasibility of parameter-dependent linearized system dynamics for a given operating point. The gain scheduler requiring online membership tests can be considered a solution to this problem [10]. Additional advanced mechanisms, including optimization [11], [12] and adaptation [13] have been adopted for the feedback gains and feed-forward terms used for the state-feedback controller. The recent online parameter estimation techniques as in [14]–[17] can alleviate the parameter dependence level of these results.

In addition to linearization techniques, nonlinear techniques, including fuzzy [18], sliding mode [19], backstepping [20], adaptation [21], and coordinate transformation [22] have been applied to solve the positioning problem by handling the nonlinearity without operating point dependency. This has required the additional feedback and feed-forward loops to incorporate the sensors, which can be addressed by utilizing the observers as in [23]–[26]. The disturbance observer (DOB) estimates the lumped disturbances from the deviation between the system model and the actual system such that it yields the feed-forward compensation terms to secure improved closed-loop robustness [27]. The combination of simple proportional-type control was presented through a back-stepping process, forming a multi-loop structure [28]. Active damping-based multi-loop controllers incorporating DOBs solved the system parameter dependence problem [29]. The elimination of the velocity sensor was accomplished using a recent DOB-based proportional-derivative (PD) controller, including the parameter-independent velocity observer [30] with convergence and closed-loop behavior analysis.

The above-mentioned results must set the current dynamics to be sufficiently fast to secure an acceptable positioning performance during both the transient and steady-state periods. During the transition periods, high current feedback gains are required for fast responsiveness. However, this high-level current feedback gain setting expands the undesirable current ripple and reduces the relative stability margin. This study considers this practical concern as the main problem in this work and proposes a solution to this problem with a few contributions given by

- Dynamic current feedback mechanism in closed form without numerical retrieval to ensure the desired performance by boosting and restoring the feedback gain value;
- Improvement of closed loop performance by using a model-free proportional-type velocity observer including a disturbance estimator;

which constitutes the novel multi-loop positioning controller adopting the active damping to the inner loop for order-reduction from the pole-zero cancellation. Section II introduces a nonlinear induction equation for MAGLEV, and Section III presents the dynamic current cutoff frequency techniques and controller design for inner/outer loops. Section IV presents the pole-zero cancellation approaches and the stability analysis of the inner and outer loops, and Section V validates the practical benefits of simulating with MATLAB/Simulink through various scenarios for position tracking and regulation. Section VI presents conclusions and future work.

II. MAGLEV NONLINEAR MOTION EQUATIONS

Fig. 1 illustrates the MAGLEV system configuration including the actuator provided by the current controller. This system is designed to maintain the desired gap (denoted as p in Fig. 1) between the magnet (attached to the train body) and the rail, which can be accomplished by the magnetic force triggered by the coil current magnitude proportional to the coil voltage. Consequently, from the perspective of system engineering, the coil voltage and position correspond to the input and output, respectively. Specifically, there is a set of state variables, p (position in m), $v_p(:= \dot{p})$ (velocity in m/s), and i_c (current in A) and control input, u (coil voltage in V), which satisfies the nonlinear dynamical relationship [13]:

$$M\ddot{p} = (M + M_L)g - K\frac{i_c^2}{p^2} + w_p, \tag{1}$$

$$L_c\dot{i}_c = -R_c i_c + u, \quad \forall t \geq 0, \tag{2}$$

where the air spring causes the load force w_p (in N) to act as an unknown mismatched disturbance. Meanwhile, the system

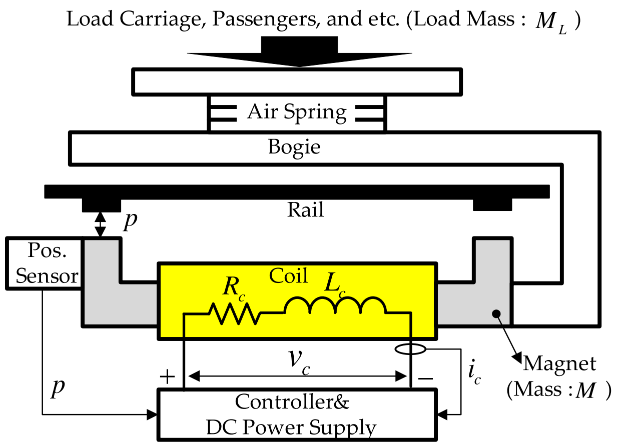

FIGURE 1. **MAGLEV system configuration.**

parameters M, M_L, g, K, R_c, and L_c represent the masses of the electromagnet and load (in kg), gravitational acceleration (9.8 in m/s^2), electromagnet force coefficient (in $N \cdot m^2/A^2$), and coil resistance and inductance (in Ω and H), respectively. Their known nominal parameter values from manufacturing are denoted as M_0, K_0, $R_{c,0}$, and $L_{c,0}$.

The application of nominal parameters to the original system dynamics (1) and (2) leads to the adoption of uncertain time-varying disturbances $\bar{w}_p$ and $\bar{w}_c$ originating from the parameter and load variations.

$$M_0\ddot{p} = M_0 g - K_0\frac{i_c^2}{p^2} + \bar{w}_p, \tag{3}$$
$$L_{c,0}\dot{i}_c = -R_{c,0}i_c + u + \bar{w}_c, \quad \forall t \geq 0, \tag{4}$$

which is used as the basis for devising the control law in the following section.

III. CONTROL LAW

This study adopts a low-pass filter (LPF) [31] as the performance index given by

$$\frac{P^*(s)}{P_{ref}(s)} = \frac{\omega_p}{s+\omega_p}, \quad \frac{I_c^*(s)}{I_{c,ref}(s)} = \frac{\omega_c}{s+\omega_c}, \quad \forall s \in \mathbb{C}, \tag{5}$$

subject to the cutoff frequencies $\omega_p = 2\pi f_p$ and $\omega_c = 2\pi f_c$ (in rad/s), where $P^*(s)$, $P_{ref}(s)$, $I_c^*(s)$, and $I_{c,ref}(s)$ represent the Laplace transforms of the desired position p^*, its reference p_{ref} (constant), coil current i_c^*, and its reference $i_{c,ref}$, respectively. The performance index (5) yields the following time-domain expressions:

$$\dot{p}^* = \omega_p(p_{ref} - p^*), \tag{6}$$
$$\dot{i}_c^* = \omega_c(i_{c,ref} - i_c^*), \quad \forall t \geq 0, \tag{7}$$

which are considered to be the desired dynamics for position and current. This derives the main control objective as exponential convergence:

$$\lim_{t\to\infty} p = p^*, \quad \lim_{t\to\infty} i_c = i_c^*. \tag{8}$$

Note that the feedback gain ω_c acting as the (inner) current loop cutoff frequency must be tuned sufficiently to enlarge the admissible range of the outer loop cutoff frequency. The large constant inner-loop cutoff frequency can magnify the unnecessary current ripple and degrade the closed-loop robustness. The proposed technique alleviates this limitation by incorporating a dynamic current feedback gain mechanism into the control action.

A. OUTER LOOP

1) VELOCITY OBSERVER

The stabilization of the second-order position dynamics (1) requires the feedback of the velocity ($v_p = \dot{p}$). The time-derivative process of the measurement p could extract the velocity information perturbed by high-frequency measurement noise, which could degrade the closed-loop accuracy. This study attempts to devise an advanced velocity observer with two merits: plant parameter independence and disturbance estimator as a replacement for the observer output error integral action, which is given by

$$\dot{\hat{p}} = \hat{v}_p + l_{v,1}e_p, \tag{9}$$
$$\dot{z}_{v_p} = -l_{v,2}z_{v_p} + l_{v,2}(\hat{v}_p + (l_{v,1} - l_{v,2})e_p), \tag{10}$$
$$\hat{v}_p = z_{v_p} + l_{v,2}e_p, \quad \forall t \geq 0, \tag{11}$$

with respect to the observer state variables $\hat{p}$ and z_{v_p}, output $\hat{v}_p$, and error $e_p = p - \hat{p}$, the velocity estimation error is defined as $e_v := v_p - \hat{v}_p$. The two design parameters $l_{v,i} > 0$ and $i = 1, 2$ determine the state update rates, the roles of which are revealed in Section IV.

2) CONTROL LAW

Consider an equivalent expression of the open-loop position dynamics (3) given by

$$\begin{aligned}\ddot{p} &= -c_p\frac{i_c^2}{p^2} + g + d_p \\ &= -\frac{c_p}{p^2}z_{ref} + \phi(i_c, z_{ref}) + g + d_p, \quad \forall t \geq 0,\end{aligned} \tag{12}$$

with the known coefficient $c_p := \frac{K_0}{M_0}$, the newly defined lumped disturbance $d_p := \frac{1}{M_0}\bar{w}_p$, the nonlinear function $\phi(i_c, z_{ref}) := \frac{c_p}{p^2}(z_{ref} - i_c^2)$, and the design variable z_{ref} to be used as the control input to stabilize the open-loop dynamics (12). The control law for updating z_{ref} is proposed as:

$$z_{ref} = \frac{p^2}{c_p}((b_{d,p} + \omega_p)\hat{v}_p - b_{d,p}\omega_p\tilde{p} + g + \hat{d}_p), \tag{13}$$

$\forall t \geq 0$, which attempts to stabilize the error $\tilde{p} := p_{ref} - p$ in accordance with the setting of the design parameters $b_{d,p} > 0$ and $\omega_p > 0$. The observer-based DOB yields the disturbance estimate $\hat{d}_p$ such that

$$\dot{z}_{d_p} = -l_{d_p}z_{d_p} - l_{d_p}^2\hat{v}_p + l_{d_p}(c_p\frac{i_c^2}{p^2} - g), \tag{14}$$
$$\hat{d}_p = z_{d_p} + l_{d_p}\hat{v}_p, \quad \forall t \geq 0, \tag{15}$$

where gain $l_{d_p} > 0$ determines the disturbance estimation rate.

Note that the observer-based feed-forward compensation term $b_{d,p}\hat{v}_p$ injects additional damping to the closed loop, where the gain $b_{d,p}$ adjusts this artificial damping intensity. Moreover, the cooperation of $b_{d,p}$ and ω_p renders the order of the closed-loop position dynamics as1 (i.e., order reduction) via pole-zero cancellation without involving any uncertainty problems. For details, see Section IV.

B. INNER LOOP

The proposed inner loop aims to devise an exponential convergent current controller, such that $\lim_{t\to\infty} i_c = i_c^*$ leadsto $\lim_{t\to\infty} \phi(i_c, z_{ref}) = 0$. For this purpose, we define the coil current reference using the outer loop control law (13) as $i_{c,ref} := \sqrt{z_{ref}}$, such that $\phi(i_{c,ref}, z_{ref})(= \phi(i_c, z_{ref})\Big|_{i_c=i_{c,ref}}) = 0$, where the outer loop control signal z_{ref} is defined in (13).

1) DYNAMIC FEEDBACK LOOP

To implement the dynamic feedback loop, consider a slight modification of (7) as

$$\dot{i}_c^* = \hat{\omega}_c(i_{c,ref} - i_c^*), \quad \forall t \geq 0, \tag{16}$$

subject to a feedback loop update mechanism [32]:

$$\dot{\hat{\omega}}_c = \kappa_{\omega_c}((\Delta i_c^*)^2 + \varsigma_{\omega_c}\tilde{\omega}_c), \quad \forall t \geq 0, \tag{17}$$

where $\Delta i_c^* := i_{c,ref} - i_c^*$; the gains $\kappa_{\omega_c} > 0$ and $\varsigma_{\omega_c} > 0$ determine the feedback gain boosting and restoring rates. The initial condition is given by $\hat{\omega}_c(0) = \omega_c$ for a constant base cutoff frequency ω_c. Issues related to stability (owing to the nonlinear term $(\Delta i_c^*)^2$) and the cutoff frequency boosting property $\hat{\omega}_c \geq \omega_c, \forall t \geq 0$, are addressed in Section IV.

2) CONTROLLER

The error $\Delta i_c := i_c^* - i_c$ yields the dynamics:

$$\Delta\dot{i}_c = -\frac{1}{L_{c,0}}u + d_c, \quad \forall t \geq 0, \tag{18}$$

where the newly defined lumped disturbance $d_c := \dot{i}_c^* + \frac{R_{c,0}}{L_{c,0}}i_c - \frac{1}{L_{c,0}}\bar{w}_c$. The control law for updating the coil voltage u is proposed as:

$$u = L_{c,0}((b_{d,c} + k_c)\Delta i_c + b_{d,c}k_c \int_0^t \Delta i_c d\tau + \hat{d}_c), \tag{19}$$

$\forall t \geq 0$, which attempts to stabilize the error $\Delta i_c = i_c^* - i_c$ in accordance with the setting of the design parameters $b_{d,c} > 0$ and $k_c > 0$. The DOB continuously adjusts the variable $\hat{d}_c$ to exponentially estimate the actual disturbance d_c such that

$$\dot{z}_{d_c} = -l_{d_c}z_{d_c} - l_{d_c}^2\Delta i_c + l_{d_c}(\frac{1}{L_{c,0}}u), \tag{20}$$

$$\hat{d}_c = z_{d_c} + l_{d_c}\Delta i_c, \quad \forall t \geq 0, \tag{21}$$

where gain $l_{d_c} > 0$ determines the disturbance estimation rate. Fig. 2 illustrates the proposed cascade feedback system structure.

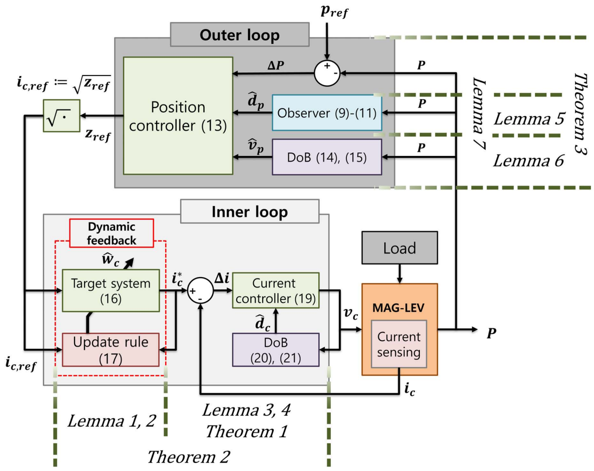

FIGURE 2. Proposed cascade feedback system structure.

Remark 1: The feed-forward compensation term $-b_{d,c}i_c$ injects additional damping to the closed-loop system where the gain $b_{d,c}$ adjusts this artificial damping intensity. Moreover, the combination of the design parameters $b_{d,c}$ and k_c renders the order of closed-loop position dynamics as 1 (i.e., order reduction) via pole-zero cancellation without involving any uncertainty problems. See Section IV for further details. ◊

IV. ANALYSIS

This section shows the accomplishment of the control objective by proving the exponential convergence (8) by considering the closed-loop error and auxiliary system dynamics. To this end, Section IV-A begins with an inner loop analysis.

A. INNER LOOP

In this section, we prove the accomplishment of the control objective for the current loop ($\lim_{t\to\infty} i_c = i_c^*$) and exponential convergence $\lim_{t\to\infty} i_c = i_{c,ref}$ such that $\lim_{t\to\infty} \phi = 0$.

1) AUXILIARY SYSTEMS

Lemma 1 and 2 analyze the closed-loop behaviors of subsystems (16) and (17).

Lemma 1: The dynamic feedback gain $\hat{\omega}_c$ always achieves a lower bound at its initial value ω_c, that is,

$$\hat{\omega}_c \geq \omega_c, \quad \forall t \geq 0. \tag{22}$$

◊

Proof: The equation $\hat{\omega}_c = e^{-\kappa_{\omega_c}\varsigma_{\omega_c}t}\omega_c + \int_0^t e^{-\kappa_{\omega_c}\varsigma_{\omega_c}(t-\tau)}(\kappa_{\omega_c}\varsigma_{\omega_c}\omega_c + \kappa_{\omega_c}(\Delta i_c^*)^2)d\tau$ satisfies the update rule (17), which has a lower bound at $\hat{\omega}_c$ due to $\kappa_{\omega_c}\varsigma_{\omega_c}\omega_c + \kappa_{\omega_c}(\Delta i_c^*)^2 > 0, \forall t \geq 0$. This completes this proof. ■

Result (22) plays an important role in proving the exponential convergence $\lim_{t\to\infty} \Delta i_c^* = i_{c,ref}$ in Theorem 2.

Lemma 2 analyzes the closed-loop stability of a time-varying system (16).

Lemma 2: The subsystem comprising (16) and (17) guarantees that there exists $a_i > 0$, $i = 1, 2$, such that

$$|\Delta i_c^*| \le a_1 e^{-a_2 t}, \quad \forall t \ge 0, \quad \forall |\Delta i_c^*| \ge \frac{2\delta_{i_{c,ref}}}{\hat{\omega}_c},$$

where $|\dot{i}_{c,ref}| \le \delta_{i_{c,ref}}$, $\forall t \ge 0$. ◊

Proof: Consider the error dynamics for (16) and (17) as follows:

$$\Delta \dot{i}_c^* = -\frac{\omega_c}{2}\Delta i_c^* + \frac{\tilde{\omega}_c}{2}\Delta i_c^* - \frac{\hat{\omega}_c}{2}\Delta i_c^* + \dot{i}_{c,ref},$$
$$\dot{\tilde{\omega}}_c = -\kappa_{\omega_c}((\Delta i_c^*)^2 + \varsigma_{\omega_c}\tilde{\omega}_c), \quad \forall t \ge 0,$$

and Lyapunov function candidate $V_1 := \frac{1}{2}(\Delta i_c^*)^2 + \frac{1}{4\kappa_{\omega_c}}\tilde{\omega}_c^2$, which results in

$$\begin{aligned}
\dot{V}_1 &= \Delta i_c^*(-\frac{\omega_c}{2}\Delta i_c^* + \frac{\tilde{\omega}_c}{2}\Delta i_c^*) \\
&\quad + \Delta i_c^*(-\frac{\hat{\omega}_c}{2}\Delta i_c^* + \dot{i}_{c,ref}) - \frac{\tilde{\omega}_c}{2}((\Delta i_c^*)^2 + \varsigma_{\omega_c}\tilde{\omega}_c) \\
&\le -\frac{\omega_c}{2}(\Delta i_c^*)^2 - \frac{\varsigma_{\omega_c}}{2}\tilde{\omega}_c^2 - (\frac{\hat{\omega}_c}{2} - \frac{\delta_{i_{c,ref}}}{|\Delta i_c^*|})(\Delta i_c^*)^2 \\
&\le -\alpha_1 V_1, \quad \forall t \ge 0, \forall |\Delta i_c^*| \ge \frac{2\delta_{i_{c,ref}}}{\hat{\omega}_c},
\end{aligned} \tag{23}$$

where $\alpha_1 := \min\{\omega_c, 2\varsigma_{\omega_c}\omega_c\}$, which completes the proof based on the comparison principle in [33]. ■

Remark 2: Considering the cutoff frequency magnification property (22), it is reasonable to assume that $\frac{2\delta_{i_{c,ref}}}{\hat{\omega}_c} \approx 0$ yielding $\dot{V}_1 \le -\alpha_1 V_1$, $\forall t \ge 0$, for some settings of κ_{ω_c} and ς_{ω_c} used for the update rule (17), which is employed in the following convergence analysis. ◊

Lemma 3 clarifies the disturbance estimation behavior from DOB (20) and (21) by investigating its output dynamics.

Lemma 3: The DOB comprising (20) and (21) ensures that:

$$\dot{\hat{d}}_c = l_{d_c}(d_c - \hat{d}_c), \quad \forall t \ge 0. \tag{24}$$

◊

Proof: Consider the time derivative of the output (21) using (20), such that

$$\begin{aligned}
\dot{\hat{d}}_c &= \dot{z}_{d_c} + l_{d_c}\Delta \dot{i}_c \\
&= -l_{d_c}(\hat{d}_c - l_{d_c}\Delta i_c) - l_{d_c}^2 \Delta i_c + l_{d_c}(\frac{1}{L_{c,0}}u) + l_{d_c}\Delta \dot{i}_c \\
&= l_{d_c}(\Delta \dot{i}_c + \frac{1}{L_{c,0}}u - \hat{d}_c) = l_{d_c}(d_c - \hat{d}_c), \quad \forall t \ge 0,
\end{aligned}$$

where the last equality is obtained using the equation $d_c = \Delta \dot{i}_c + \frac{1}{L_{c,0}}u$ from (18). This completes this proof. ■

Remark 3: Two implications can be derived from the results in (24):

- (DOB gain tuning) $\frac{\hat{D}_c(s)}{D_c(s)} = \frac{l_{d_c}}{s+l_{d_c}}$ with $D_c(s)$ and $\hat{D}_c(s)$ representing the Laplace transforms of d_c and $\hat{d}_c$, respectively, which indicates that the DOB gain can be tuned as the cutoff frequency ($l_{d_c} = 2\pi f_{d_c}$ rad/s) of LPF from the input d_c to the output $\hat{d}_c$.
- (estimation error dynamics) the disturbance estimation error dynamics for $e_{d_c} := d_c - \hat{d}_c$:

$$\dot{e}_{d_c} = -l_{d_c}e_{d_c} + w_{d_c}, \quad \forall t \ge 0, \tag{25}$$

with $w_{d_c} := \dot{d}_c$ and $|w_{d_c}| \le \delta_{d_c}$, $\forall t \ge 0$, which is used in the following convergence analysis.

◊

2) CONTROL LAW

As can be seen from the combination of (18) and (17), the inner loop system seems to be governed by second-order dynamics owing to the first-order integral action of the control law (19). Interestingly, the combination of the active damping coefficient $b_{d,c}$ and the design parameter structure results in first-order closed-loop dynamics owing to the order reduction property of active damping. For details, refer to Lemma 4.

Lemma 4: The inner-loop system shown in Fig. 2 controls the coil current, such that

$$\Delta \dot{i}_c = -k_c \Delta i_c + e_{d_c} + e_{d_c,F}, \tag{26}$$

with filtering dynamics

$$\dot{e}_{d_c,F} = -a_{c,1}e_{d_c,F} - a_{c,2}e_{d_c}, \quad \forall t \ge 0, \tag{27}$$

for some $a_{c,i} > 0$, $i = 1, 2$. ◊

Proof: Substituting (19) into (18) yields the closed-loop current dynamics:

$$\begin{aligned}
\Delta \dot{i}_c &= -b_{d,c}\Delta i_c + k_c(r - \Delta i_c) + b_{d,c}k_c\int_0^t (r - \Delta i_c)d\tau \\
&\quad + e_{d_c}, \quad \forall t \ge 0,
\end{aligned}$$

where $r = 0$ and $e_{d_c} := d_c - \hat{d}_c$. Its vector form for $\boldsymbol{x}_c := \begin{bmatrix} \Delta i_c & \zeta_c \end{bmatrix}^T$ with $\zeta_c := b_{d,c}k_c\int_0^t \Delta i_c d\tau$ is given by

$$\dot{\boldsymbol{x}}_c = \boldsymbol{A}_c\boldsymbol{x}_c + \boldsymbol{b}_{c,1}r + \boldsymbol{b}_{c,2}e_{d_c}, \tag{28}$$
$$y_c = \boldsymbol{c}_c\boldsymbol{x}_c (= \Delta i_c), \quad \forall t \ge 0, \tag{29}$$

whose matrices are defined as $\boldsymbol{A}_c := \begin{bmatrix} -(b_{d,c}+k_c) & 1 \\ -b_{d,c}k_c & 0 \end{bmatrix}$, $\boldsymbol{b}_{c,1} := \begin{bmatrix} k_c & b_{d,c}k_c \end{bmatrix}^T$, $\boldsymbol{b}_{c,2} := \begin{bmatrix} 1 & 0 \end{bmatrix}^T$, and $\boldsymbol{c}_c := \begin{bmatrix} 1 & 0 \end{bmatrix}$. This yields the input-output relationship through the Laplace transform to the system of (28) and (29) as

$$\begin{aligned}
\Delta I_c(s) &= \boldsymbol{c}_c(s\boldsymbol{I} - \boldsymbol{A}_c)^{-1}\boldsymbol{b}_{c,1}R(s) \\
&\quad + \boldsymbol{c}_c(s\boldsymbol{I} - \boldsymbol{A}_c)^{-1}\boldsymbol{b}_{c,2}E_{d_c}(s), \\
&= \frac{k_c}{s+k_c}R(s) + \frac{s}{(s+k_c)(s+b_{d,c})}E_{d_c}(s), \\
&\quad \forall s \in \mathbb{C},
\end{aligned} \tag{30}$$

where the combination of design parameters $b_{d,c}$ and k_c results in order reduction given as follows:

$$\boldsymbol{c}_c(s\boldsymbol{I} - \boldsymbol{A}_c)^{-1}\boldsymbol{b}_{c,1}R(s) = \frac{k_c(s+b_{d,c})}{(s+k_c)(s+b_{d,c})} = \frac{k_c}{s+k_c},$$

$\forall s \in \mathbb{C}$. Then, it follows from (30) and the relationship $\frac{s}{(s+b_{d,c})} = 1 - \frac{b_{d,c}}{s+b_{d,c}}$ that:

$$(s+k_c)\Delta I_c(s) = k_c R(s) + E_{d_c}(s) + E_{d_c,F}(s), \quad \forall s \in \mathbb{C},$$

where $E_{d_c,F} = -\frac{b_{d,c}}{s+b_{d,c}}E_{d_c}(s)$. This completes the proof of this lemma by considering the inverse Laplace transform on both sides above. ■

Theorems 1 and 2 present the main results of this subsection. Theorem 1 provides a property related to the control objective accomplishment by employing the subsystem analysis results.

Theorem 1: The inner-loop system shown in Fig. 2 guarantees that there exist $b_i > 0$, $i = 1, 2$,

$$|\Delta i_c| \le b_1 e^{-b_2 t}, \quad \forall t \ge 0, \quad \forall |e_{d_c}| \ge \frac{2\delta_{d_c}}{l_{d_c}}. \tag{31}$$

◊

Proof: Consider the positive definite function $V_{e_{d_c}} := \frac{1}{2}e_{d_c,F}^2 + \frac{\zeta_{d_c}}{2}e_{d_c}^2$ with $\zeta_{d_c} > 0$ whose time derivative is obtained by (using (25), (27), and Young's inequality (e.g., $xy \le \frac{\epsilon}{2}x^2 + \frac{1}{2\epsilon}y^2$, $\forall \epsilon > 0$))

$$\begin{aligned}\dot{V}_{e_{d_c}} &= e_{d_c,F}(-a_{c,1}e_{d_c,F} - a_{c,2}e_{d_c}) - \frac{\eta_{d_c}l_{d_c}}{2}e_{d_c}^2 \\ &\quad - \eta_{d_c}(\frac{l_{d_c}}{2}e_{d_c}^2 - e_{d_c}w_{d_c}) \\ &\le -\frac{a_{c,1}}{2}e_{d_c,F}^2 - \frac{1}{2}(\eta_{d_c}l_{d_c} - \frac{a_{c,2}^2}{a_{c,1}})e_{d_c}^2,\end{aligned}$$

$\forall t \ge 0, \forall |e_{d_c}| \ge \frac{2\delta_{d_c}}{l_{d_c}}$. Setting $\zeta_{d_c} = \frac{1}{l_{d_c}}(\frac{a_{c,2}^2}{a_{c,1}} + 1)$, we obtain:

$$\begin{aligned}\dot{V}_{e_{d_c}} &\le -\frac{a_{c,1}}{2}e_{d_c,F}^2 - \frac{1}{2}e_{d_c}^2 \\ &\le -\alpha_{e_{d_c}}V_{e_{d_c}}, \quad \forall t \ge 0, \quad \forall |e_{d_c}| \ge \frac{2\delta_{d_c}}{l_{d_c}}, \end{aligned} \tag{32}$$

where $\alpha_{e_{d_c}} := \min\{a_{c,1}, \frac{1}{\zeta_{d_c}}\}$, The result (26) and inequality (32) render the positive definite function $V_{\Delta i_c} := \frac{1}{2}\Delta i_c^2 + \eta_{e_{d_c}}V_{e_{d_c}}$ with $\eta_{e_{d_c}} > 0$ as follows:

$$\begin{aligned}\dot{V}_{\Delta i_c} &= \Delta i_c(-k_c\Delta i_c + e_{d_c} + e_{d_c,F}) + \eta_{e_{d_c}}\dot{V}_{e_{d_c}} \\ &\le -\frac{k_c}{3}\Delta i_c^2 - (\eta_{e_{d_c}}\alpha_{e_{d_c}} - \frac{8}{3k_c}\max\{1, \frac{1}{\zeta_{d_c}}\})V_{e_{d_c}},\end{aligned}$$

$\forall t \ge 0$, $\forall |e_{d_c}| \ge \frac{2\delta_{d_c}}{l_{d_c}}$. The coefficient $\eta_{e_{d_c}} := \frac{1}{\alpha_{e_{d_c}}}(\frac{8}{3k_c}\max\{1, \frac{1}{\zeta_{d_c}}\} + 1)$ gives the upper bound of $\dot{V}_{\Delta i_c}$ as:

$$\begin{aligned}\dot{V}_{\Delta i_c} &\le -\frac{k_c}{2}\Delta i_c^2 - V_{e_{d_c}} \\ &\le -\alpha_{\Delta i_c}V_{\Delta i_c}, \quad \forall t \ge 0, \quad \forall |e_{d_c}| \ge \frac{2\delta_{d_c}}{l_{d_c}}, \end{aligned} \tag{33}$$

where $\alpha_{\Delta i_c} := \min\{k_c, \frac{1}{\eta_{e_{d_c}}}\}$. This confirms the result of this theorem by using the comparison principle in [33]. ■

The result (31) shows exponential convergence (control objective (8)):

$$\lim_{t\to\infty} i_c = i_c^*$$

with the condition $\frac{2\delta_{d_c}}{l_{d_c}} \approx 0$ (DOB gain setting), which concludes the control objective (8) and is assumed to derive the useful inequality from (33):

$$\dot{V}_{\Delta i_c} \le -\alpha_{\Delta i_c}V_{\Delta i_c}, \quad \forall t \ge 0, \tag{34}$$

for the remaining convergence analysis.

Theorem 2 proves the exponential convergence of the actual coil current error $\tilde{i}_c := i_{c,ref} - i_c$ based on the inequality (34), which acts as the rationale for assuming that $\lim_{t\to\infty}\phi = 0$.

Theorem 2: The inner-loop system shown in Fig. 2 guarantees the property:

$$\lim_{t\to\infty} i_c = i_{c,ref}, \tag{35}$$

exponentially. ◊

Proof: The actual error $\tilde{i}_c = i_{c,ref} - i_c$ satisfies $\tilde{i}_c = \Delta i_c^* + \Delta i_c$ (equivalently, $\Delta i_c^* = \tilde{i}_c - \Delta i_c$), which shows that:

$$\begin{aligned}\dot{\tilde{i}}_c &= \Delta\dot{i}_c^* + \Delta\dot{i}_c \\ &= -\hat{\omega}_c\Delta i_c^* + \dot{i}_{c,ref} - k_c\Delta i_c + \mathbf{1}^T\boldsymbol{e}_{d_c} \\ &= -\hat{\omega}_c\tilde{i}_c + c\Delta i_c + \mathbf{1}^T\boldsymbol{e}_{d_c} + \dot{i}_{c,ref}, \quad \forall t \ge 0,\end{aligned}$$

where $c := \hat{\omega}_c - k_c$. Consequently, the positive definite function $V_c := \frac{1}{2}\tilde{i}_c^2 + \eta_{\Delta i_c}V_{\Delta i_c}$ with $\eta_{\Delta i_c} > 0$ shows that

$$\begin{aligned}\dot{V}_c &= \tilde{i}_c(-\frac{\hat{\omega}_c}{2}\tilde{i}_c + c\Delta i_c + \mathbf{1}^T\boldsymbol{e}_{d_c}) - \tilde{i}_c(\frac{\hat{\omega}_c}{2}\tilde{i}_c - \dot{i}_{c,ref}) \\ &\quad + \eta_{\Delta i_c}\dot{V}_{\Delta i_c} \\ &\le -\frac{\omega_c}{3}\tilde{i}_c^2 - (\eta_{\Delta i_c}\alpha_{\Delta i_c} - \frac{4\bar{c}^2}{3\omega_c} - \frac{4}{\omega_c\eta_{e_{dc}}})V_{\Delta i_c} \\ &\quad - (\frac{\hat{\omega}_c}{2} - \frac{\delta_{i_{c,ref}}}{|\tilde{i}_c|})\tilde{i}_c^2 \\ &\le -\frac{\omega_c}{3}\tilde{i}_c^2 - V_{\Delta i_c}, \quad \forall t \ge 0, \quad \forall |\tilde{i}_c| \ge \frac{2\delta_{i_{c,ref}}}{\hat{\omega}_c},\end{aligned}$$

where the first inequality is obtained from the result (22) and Young's inequality, and the coefficient $\eta_{\Delta i_c} := \frac{1}{\alpha_{\Delta i_c}}(\frac{4\bar{c}^2}{3\omega_c} + \frac{4}{\omega_c\eta_{e_{d_c}}} + 1)$ justifies the second inequality. The assumption made in Remark 2 concludes that

$$\dot{V}_c \le -\alpha_c V_c, \quad \forall t \ge 0, \tag{36}$$

where $\alpha_c := \min\{\frac{2\omega_c}{3}, \frac{1}{\eta_{\Delta i_c}}\}$, which completes the proof. ■

Remark 4: The result (35) implies the exponential convergence of the nonlinear function $\phi(i_c, z_{ref})$ such that $\lim_{t\to\infty}\phi(i_c, z_{ref}) = \phi(i_{c,ref}, z_{ref}) = 0$, which provides a rationale for assuming that

$$\dot{\phi} = -\alpha_\phi\phi, \quad \forall t \ge 0, \tag{37}$$

for some $\alpha_\phi > 0$, corresponding to one of the main results in this subsection. ◊

B. WHOLE LOOP

This section aims to prove the accomplishment of the main control objective ($\lim_{t\to\infty} p = p^*$) by analyzing the outer loop dynamics and employing the main inner loop analysis result (37).

1) OUTER LOOP AUXILIARY SYSTEMS

Lemma 5 clarifies the velocity estimation behavior of the observer (9)–(11) by investigating its output dynamics.

Lemma 5: The observer comprising (9)–(11) ensures that:

$$\dot{\hat{v}}_p = l_{v,2}(v_p - \hat{v}_p), \quad \forall t \geq 0, \tag{38}$$

◊

Proof: Consider the time derivative of the observer output (11) along (9) and (10) such that

$$\begin{aligned}\dot{\hat{v}}_p &= \dot{z}_{v_p} + l_{v,2}\dot{e}_p \\ &= -l_{v,2}(\hat{v}_p - l_{v,2}e_p) + l_{v,2}(\hat{v}_p + (l_{v,1} - l_{v,2})e_p) \\ &\quad + l_{v,2}(e_v - l_{v,1}e_p) = l_{v,2}e_v, \quad \forall t \geq 0,\end{aligned}$$

This completes the proof. ■

Remark 5: Two implications can be derived from the results in (38):

- (observer gain tuning) $\frac{\hat{V}_p(s)}{V_p(s)} = \frac{l_{v,2}}{s+l_{v,2}}$ with $V_p(s)$ and $\hat{V}_p(s)$ representing the Laplace transforms of v_p and $\hat{v}_p$, respectively, which indicates that the observer $l_{v,2}$ can be tuned as the cutoff frequency ($l_{v,2} = 2\pi f_{v,2}$ rad/s) of LPF from the input v_p to the output $\hat{v}_p$. After this setting for $l_{v,2}$, the remaining observer gain $l_{v,1}$ should be adjusted for e_p and e_v to be convergent as fast as possible.
- (estimation error dynamics) Consider the desired velocity estimate v_p^* such that $\dot{e}_v^* = -l_{v,2}e_v^*$ with $e_v^* := v_p - \hat{v}_p^*$. Then, the performance error $e := \hat{v}_p^* - \hat{v}_p$ satisfies $\dot{e} = \dot{\hat{v}}_p^* - \dot{\hat{v}}_p = l_{v,2}e_v^* + \dot{v}_p - l_{v,2}e_v = -l_{v,2}e + w_{v_p}$ with $w_{v_p} := \dot{v}_p$ and $|w_{v_p}| \leq \delta_{v_p}, \forall t \geq 0$, which yields for $V := \frac{1}{2}e^2$ that $\dot{V} = -\frac{l_{v,2}}{2}e^2 + e(-\frac{l_{v,2}}{2}e + w_{v_p}) \leq -\frac{l_{v,2}}{2}e^2$, $\forall t \geq 0, \forall |e| \geq \frac{2\delta_{v_p}}{l_{v,2}}$. This validates the exponential convergence $\lim_{t\to\infty}\hat{v}_p = \hat{v}_p^*$ (performance recovery) with the observer gain setting $\frac{2\delta_{v_p}}{l_{v,2}} \approx 0$. Therefore, it is reasonable to assume that

$$\dot{e}_v = -l_{v_2}e_v, \quad \forall t \geq 0, \tag{39}$$

by the proposed observer (9)-(11), which is used in the remaining convergence analysis.

◊

Similar to the proof of Lemma 3, Lemma 6 derives the disturbance estimation behavior of the observer-based DOB (14) and (15) using dynamics (39).

Lemma 6: The DOB driven by (14) and (15) ensures that:

$$\dot{\hat{d}}_p = l_{d_p}(d_p - \hat{d}_p) + l_{d_p}l_{v,2}e_v, \quad \forall t \geq 0. \tag{40}$$

◊

Proof: The proof is omitted because it is identical to the proof of Lemma 3 using the outputs (15), (14), and $d_p = \ddot{x} + c_p\frac{i_c^2}{p^2} - g$ (from (12), and (39)). ■

Remark 6: Two implications can be derived from the result (40) by setting $e_v = 0$.

- (DOB gain tuning) $\frac{\hat{D}_p(s)}{D_p(s)} = \frac{l_{d_p}}{s+l_{d_p}}$ with $D_p(s)$ and $\hat{D}_p(s)$ representing the Laplace transforms of d_p and $\hat{d}_p$, respectively, which indicates that the DOB gain can be tuned as the cutoff frequency ($l_{d_p} = 2\pi f_{d_p}$ rad/s) of LPF from the input d_p to the output $\hat{d}_p$.
- (estimation error dynamics) the disturbance estimation error dynamics for $e_{d_p} := d_p - \hat{d}_p$:

$$\dot{e}_{d_p} = -l_{d_p}e_{d_p} - l_{d_p}l_{v,2}e_v + w_{d_p}, \quad \forall t \geq 0, \tag{41}$$

with $w_{d_p} := \dot{d}_p$ and $|w_{d_p}| \leq \delta_{d_p}, \forall t \geq 0$, which is used in the following convergence analysis.

◊

2) WHOLE SYSTEM DYNAMICS

As can be seen from the combination of (12) and (13), the outer-loop system seems to be governed by second-order dynamics. Interestingly, the combination of the active damping coefficient $b_{d,p}$ and the design parameter structure results in first-order closed-loop dynamics, owing to the order reduction property. For details, refer to Lemma 7.

Lemma 7: The proposed outer-loop system, shown in Fig. 2 controls the position such that

$$\dot{p} = \omega_p\tilde{p} + e_F, \tag{42}$$

with filtering dynamics

$$\dot{e}_F = -a_{p,1}e_F + a_{p,2}(qe_v + \phi + e_{d_p}), \quad \forall t \geq 0, \tag{43}$$

for some $a_{p,i} > 0$, $i = 1, 2$, and $q > 0$. ◊

Proof: Substituting (13) into (12) yields the closed-loop position dynamics:

$$\begin{aligned}\ddot{p} &= -(b_{d,p} + \omega_p)\hat{v}_p + b_{d,p}\omega_p\tilde{p} + e_{d_p} + \phi \\ &= -b_{d,p}\dot{p} + \omega_p(\dot{p}_{ref} - \dot{p}) + b_{d,p}\omega_p\tilde{p} + qe_v + \phi + e_{d_p},\end{aligned}$$

$\forall t \geq 0$, where $q := b_{d,p} + \omega_p$ and $e_{d_p} := d_p - \hat{d}_p$, which shows that:

$$\begin{aligned}\dot{p} &= -b_{d,p}p + \omega_p(p_{ref} - p) + b_{d,p}\omega_p\int_0^t \tilde{p}d\tau \\ &\quad + w_{e_v} + w_\phi + w_{e_{d_p}}, \quad \forall t \geq 0,\end{aligned}$$

with $w_{e_v} := \int_0^t qe_v d\tau$, $w_\phi := \int_0^t \phi d\tau$, and $w_{e_{d_p}} := \int_0^t e_{d_p}d\tau$. This gives an equivalent vector form for $\boldsymbol{x}_p := \begin{bmatrix} p & \zeta_p \end{bmatrix}^T$ with $\zeta_p := b_{d,p}\omega_p\int_0^t \tilde{p}d\tau$:

$$\dot{\boldsymbol{x}}_p = \boldsymbol{A}_p\boldsymbol{x}_p + \boldsymbol{b}_{p,1}p_{ref} + \boldsymbol{b}_{p,2}(w_{e_v} + w_\phi + w_{e_{d_p}}), \tag{44}$$

$$y_p = \boldsymbol{c}_p\boldsymbol{x}_p (= p), \quad \forall t \geq 0, \tag{45}$$

whose matrices are defined as $\boldsymbol{A}_p := \begin{bmatrix} -(b_{d,p} + \omega_p) & 1 \\ -b_{d,p}\omega_p & 0 \end{bmatrix}$, $\boldsymbol{b}_{p,1} := \begin{bmatrix} \omega_p & b_{d,p}\omega_p \end{bmatrix}^T$, $\boldsymbol{b}_{p,2} := \begin{bmatrix} 1 & 0 \end{bmatrix}^T$, and $\boldsymbol{c}_p := \begin{bmatrix} 1 & 0 \end{bmatrix}$. The remaining proof is omitted since it is identical to the proof of Lemma 4 using the representation of (44) and (45). ■

Theorem 3 concludes this section by proving a closed-loop property related to the main control objective (8) based on the results of (37), (42), and (43).

Theorem 3: The multi-loop feedback system shown in Fig. 2 guarantees that there exists $c_i > 0$, $i = 1, 2$ such that

$$|\Delta p| \le c_1 e^{-c_2 t}, \quad \forall t \ge 0, \quad \forall |e_{d_p}| \ge \frac{2\delta_{d_p}}{l_{d_p}}, \tag{46}$$

with a performance error $\Delta p := p^* - p$. ♢

Proof: The definition $\boldsymbol{e}_\phi := \begin{bmatrix} e_F & \phi \end{bmatrix}^T$ reads the dynamics from (37) and (39) that

$$\dot{\boldsymbol{e}}_\phi = \boldsymbol{A}_\phi \boldsymbol{e}_\phi + \boldsymbol{b}_{\phi,1} e_{d_p} + \boldsymbol{b}_{\phi,2} e_v, \quad \forall t \ge 0, \tag{47}$$

with $\boldsymbol{A}_\phi := \begin{bmatrix} -a_{p,1} & a_{p,2} \\ 0 & -\alpha_\phi \end{bmatrix}$, $\boldsymbol{b}_{\phi,1} := \begin{bmatrix} a_{p,2} \\ 0 \end{bmatrix}$, and $\boldsymbol{b}_{\phi,2} := \begin{bmatrix} a_{p,2}q \\ 0 \end{bmatrix}$. The stability of system matrix $\boldsymbol{A}_\phi$ solves the matrix equation $\boldsymbol{A}_\phi^T \boldsymbol{P}_\phi + \boldsymbol{P}_\phi \boldsymbol{A}_\phi = -\boldsymbol{I}$ for an unique $\boldsymbol{P}_\phi > \boldsymbol{0}$, which turns the positive definite function

$$V_\phi := \frac{1}{2}\boldsymbol{e}_\phi^T \boldsymbol{P}_\phi \boldsymbol{e}_\phi + \frac{\eta_1}{2} e_{d_p}^2 + \frac{\eta_2}{2} e_v^2, \quad \eta_i > 0, i = 1, 2, \quad \forall t \ge 0,$$

into (using Young's inequality)

$$\begin{aligned} \dot{V}_\phi &= \boldsymbol{e}_\phi^T \boldsymbol{P}_\phi (\boldsymbol{A}_\phi \boldsymbol{e}_\phi + \boldsymbol{b}_{\phi,1} e_{d_p} + \boldsymbol{b}_{\phi,2} e_v) \\ &\quad + \eta_1 e_{d_p}(-\frac{l_{d_p}}{2} e_{d_p} - l_{d_p} l_{v,2} e_v) - \eta_2 l_{v_2} e_v^2 \\ &\quad - \eta_1 (\frac{l_{d_p}}{2} e_{d_p}^2 - e_{d_p} w_{d_p}) \\ &\le -\frac{1}{3}\|\boldsymbol{e}_\phi\|^2 - (\frac{\eta_1 l_{d_p}}{2} - \frac{3\|\boldsymbol{P}_\phi\|^2 \|\boldsymbol{b}_{\phi,1}\|^2}{4} - \frac{1}{2}) e_{d_p}^2 \\ &\quad - (\eta_2 l_{v_2} - \frac{3\|\boldsymbol{P}_\phi\|^2 \|\boldsymbol{b}_{\phi,2}\|^2}{4} - \frac{\eta_1^2 l_{d_p}^2 l_{v,2}^2}{2}) e_v^2, \end{aligned}$$

$\forall t \ge 0$, $\forall |e_{d_p}| \ge \frac{2\delta_{d_p}}{l_{d_p}}$. Settings $\eta_1 := \frac{2}{l_{d_p}}(\frac{3\|\boldsymbol{P}_\phi\|^2 \|\boldsymbol{b}_{\phi,1}\|^2}{4} + 1)$ and $\eta_2 := \frac{1}{l_{v_2}}(\frac{3\|\boldsymbol{P}_\phi\|^2 \|\boldsymbol{b}_{\phi,1}\|^2}{4} + \frac{\eta_1^2 l_{d_p}^2 l_{v,2}^2}{2} + \frac{1}{2})$ yield

$$\begin{aligned} \dot{V}_\phi &\le -\frac{1}{3}\|\boldsymbol{e}_\phi\|^2 - \frac{1}{2} e_{d_p}^2 - \frac{1}{2} e_v^2 \\ &\le -\alpha_{e_\phi} V_\phi, \quad \forall t \ge 0, \quad \forall |e_{d_p}| \ge \frac{2\delta_{d_p}}{l_{d_p}}, \end{aligned} \tag{48}$$

where $\alpha_{e_\phi} := \min\{\frac{2}{3\lambda_{min}(\boldsymbol{P}_\phi)}, \frac{1}{\eta_1}, \frac{1}{\eta_2}\}$. Now, consider the dynamics for the performance error $\Delta p = p^* - p$ as (using (6) and (42)):

$$\Delta \dot{p} = -\omega_p \Delta p - \boldsymbol{e}_1^T \boldsymbol{e}_\phi, \quad \forall t \ge 0,$$

where $\boldsymbol{e}_1 := \begin{bmatrix} 1 & 0 \end{bmatrix}^T$, which gives the time derivative of the composite-type Lyapunov function candidate $V_{\Delta p} := \frac{1}{2}\Delta p^2 + \eta_\phi V_\phi$ with $\eta_\phi > 0$ (together with (48) and Young's inequality).

$$\begin{aligned} \dot{V}_{\Delta p} &= \Delta p(-\omega_p \Delta p - \boldsymbol{e}_1^T \boldsymbol{e}_\phi) + \eta_\phi \dot{V}_\phi \\ &\le -\frac{\omega_p}{2}\Delta p^2 - (\eta_\phi \alpha_\phi - \frac{1}{\omega_p \lambda_{min}(\boldsymbol{P}_\phi)}) V_\phi \\ &\le -\alpha_{\Delta p} V_{\Delta p}, \quad \forall t \ge 0, \quad \forall |e_{d_p}| \ge \frac{2\delta_{d_p}}{l_{d_p}}, \end{aligned}$$

with the setting $\eta_\phi := \frac{1}{\alpha_\phi}(\frac{1}{\omega_p \lambda_{min}(\boldsymbol{P}_\phi)} + 1)$ and a positive constant $\alpha_{\Delta p} := \min\{\omega_p, \frac{1}{\eta_\phi}\}$. This completes this proof. ■

The result (46) shows exponential convergence (control objective (8)):

$$\lim_{t \to \infty} p = p^*$$

with the DOB gain setting $\frac{2\delta_{d_p}}{l_{d_p}} \approx 0$, which concludes control objective (8).

V. SIMULATIONS

This section demonstrates the performance improvement from the closed-loop analysis results in Section IV using numerical simulations based on MATLAB/Simulink. The nonlinear differential equations (1) and (2) emulated the MAGLEV system dynamics for the position, velocity, and coil current through Simulink programming in a continuous time setting, where the system coefficients are set to $M = 725\ kg$, $M_L = 1000\ kg$ (initial load), $K = 5.45 \times 10^{-3}\ N \cdot m^2/A^2$, $R_c = 4.4\ \Omega$, and $L_c = 908\ mH$. These values were obtained from an actual experimental test bed in [13]. The control algorithms were coded using C programming in the S-function environment, which was executed for each sampling and control period 1 ms and implemented using the nominal system parameter setting $M_0 = 0.7\,M$, $K_0 = 1.5\,K$, $R_{c,0} = 1.3\,R_c$, and $L_{c,0} = 0.5\,L_c$.

The design parameter tuning results for the proposed controller are summarized as: (outer loop) $f_p = 0.5$ Hz (for $\omega_p = 2\pi 0.5$ rad/s), $b_{d,p} = 2000$, $f_{d_p} = 300$ Hz (for $l_{d_p} = 2\pi 300$ rad/s), $f_{v,1} = 200$ Hz (for $l_{v,1} = 2\pi 200$ rad/s), $f_{v,2} = 1000$ Hz (for $l_{v,2} = 2\pi 1000$ rad/s), (inner loop) $f_c = 8$ Hz (for $\hat{\omega}_c(0) = \omega_c = 2\pi 8$ rad/s), $b_{d,c} = 2000$, $k_c = 1900$, $f_{d_c} = 1000$ Hz (for $l_{d_c} = 2\pi 1000$ rad/s), $\kappa_{\omega_c} = 5$, and $\varsigma_{\omega_c} = \frac{1}{\kappa_{\omega_c}}$. A comparison analysis was conducted to clarify the practical advantage with the back-stepping controller (BSC) compensated by the active damping terms and DOBs such that: (position loop) $v_{p,ref} = \omega_p \tilde{p}$, (velocity loop) $i_{c,ref} = \sqrt{\frac{p^2}{c_p}(b_{d,v} v_p - \omega_v \tilde{v}_p - b_{d,v}\omega_v \int_0^t \tilde{v}_p d\tau + g + \hat{d}_v)}$ ($\tilde{v}_p := v_{p,ref} - v_p$), $\dot{z}_v = -l_{d_p} z_v - l_{d_p}^2 v_p + l_{d_p}(c_p \frac{i_c^2}{p^2} - g)$, $\hat{d}_v = z_v + l_{d_p} v_p$, (current loop) $u = L_{c,0}(-b_{d,c} i_c + \omega_c \tilde{i}_c + b_{d,c}\omega_c \int_0^t \tilde{i}_c d\tau - \hat{d}_c)$, $\dot{z}_c = -l_{d_c} z_c - l_{d_c}^2 i_c - l_{d_c}(\frac{u}{L_{c,0}})$, and $\hat{d}_c = z_c + l_{d_c} i_c$. Numerous shared design parameters, such as ω_p, ω_c, l_{d_p}, l_{d_c}, $b_{d,v}$, and $b_{d,c}$ were chosen to be the same as those of the proposed controller. The velocity cutoff frequency was set as $f_v = 5$ Hz (for $\omega_v = 2\pi 5$ rad/s) for the best performance.

The load force w_p was set to be sinusoidal such that $w_p = 2 \times 10^3 \sin(2\pi 3t)$, $\forall t \ge 0$, for all simulations to verify the disturbance rejection performance.

A. POSITION TRACKING COMPARISON

This subsection tests the closed-loop improvement under the position-tracking mission for the pulse reference with a minimum 1 cm and a maximum 3 cm, which were performed three times with increasing position-loop cutoff

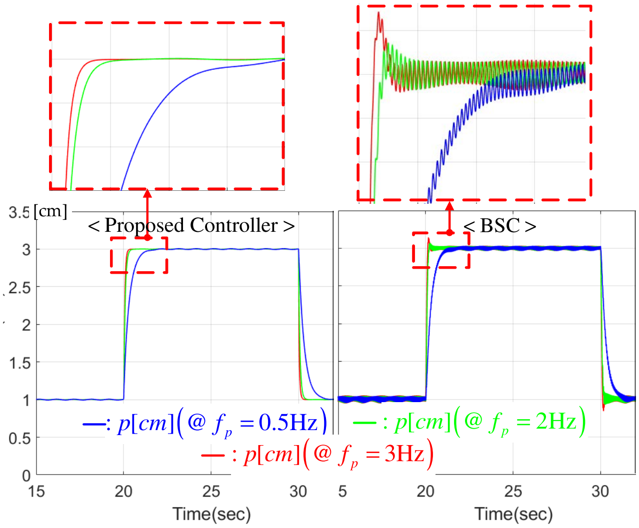

FIGURE 3. Position tracking performance changes for cutoff frequencies $f_p = 0.5$, 2, and 3 Hz.

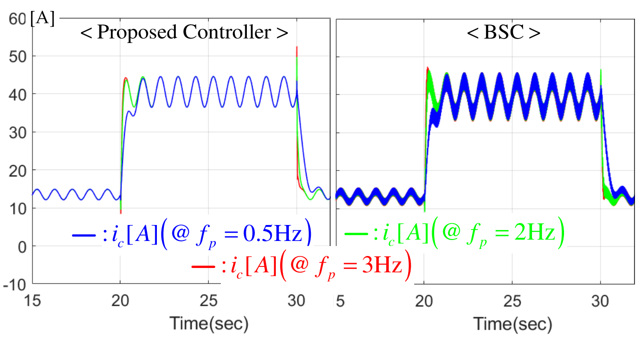

FIGURE 4. Coil current response comparison under position tracking test for cutoff frequencies $f_p = 0.5$, 2, and 3 Hz.

frequencies of $f_p = 0.5$, 2, and 3 Hz. Fig. 3 presents the closed-loop position responses driven by the proposed and BSC techniques; the proposed control action successfully eliminates the overshoots while maintaining the desirable closed-loop performance given as the cutoff frequency f_p, which comes from the dynamic feedback gain behavior presented in the right side of Fig. 5. Fig. 4 compares the coil current responses under this tracking mission. Unlike the BSC, the proposed controller featuring the dynamic cutoff frequency mechanism removes current ripples, unlike the BSC. This merit would lead to a power efficiency improvement in actual implementation during steady-state operation. The proposed observer estimates the actual velocity with satisfactory estimation error elimination behavior, which is presented on the left side of Fig. 5. The DOB responses are shown in Fig. 6, and their rapid disturbance estimation performance contributes to this significant improvement in the closed-loop performance.

B. POSITION REGULATION COMPARISON

This subsection changes the test mode by adopting a constant position reference of 2 cm, three sudden load mass increases,

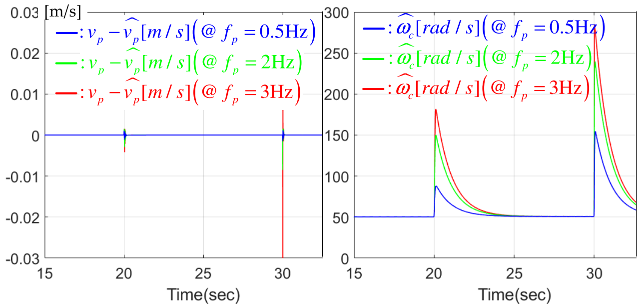

FIGURE 5. Velocity estimation error and current cutoff frequency responses under position tracking test for cutoff frequencies $f_p = 0.5$, 2, and 3 Hz.

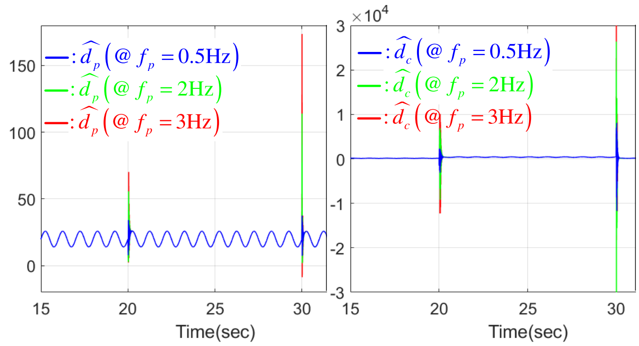

FIGURE 6. DOB responses under position tracking test for cutoff frequencies $f_p = 0.5$, 2, and 3 Hz.

and restoring scenarios such that $M_L = 1000$ (initial load mass) $\rightarrow$ 2000/3000/4000 $\rightarrow$ 1000 kg. The remaining controller design parameters were kept identical to those in the previous test with the initial setting of the position cutoff frequency $f_p = 0.5$ Hz. Fig. 7 confirms a significant closed-loop performance improvement from both the quantitative and qualitative perspectives. The proposed technique reduces the position ripple level and results in consistent performance despite the different operating conditions in the first two load mass variation scenarios. In the third scenario, the BSC fails to stabilize the closed-loop system when the load mass is suddenly increased from $M_L = 1000$ to 4000 kg; however, stabilization was successful via the proposed controller. As shown in Fig. 8, coil current ripple reduction was obtained by the proposed technique. The dynamic current cutoff frequency magnification properties presented in Fig. 9 offers these benefits.

C. NUMERICAL PERFORMANCE COMPARISON RESULTS

This subsection presents the numerical performance comparison results for evaluating the position error and current ripple-reduction levels. For this purpose, the performance metric is defined as

$$J = \sqrt{\int_0^\infty |p_{ref} - p|^2 + |i_{c,ref} - i_c|^2 dt},$$

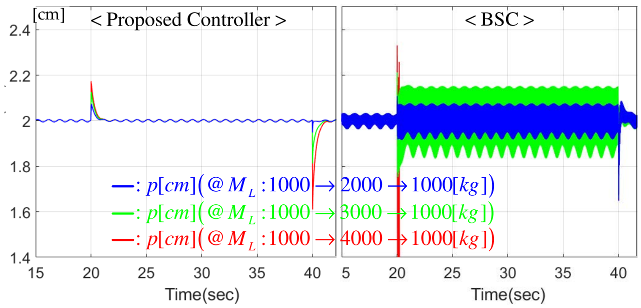

FIGURE 7. Position regulation performance changes for three load variation scenarios; M_L : 1000 → 2000/3000/4000 → 1000 *kg*.

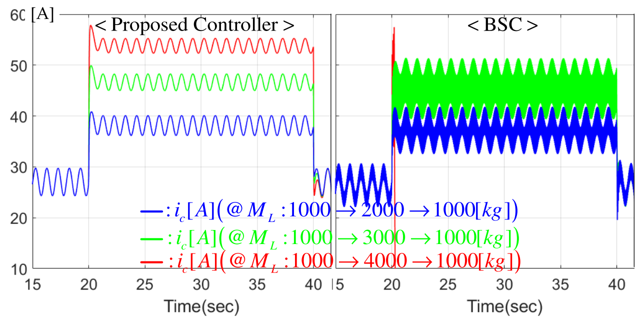

FIGURE 8. Coil current response comparison under position test for three load variation scenarios; M_L : 1000 → 2000/3000/4000 → 1000 *kg*.

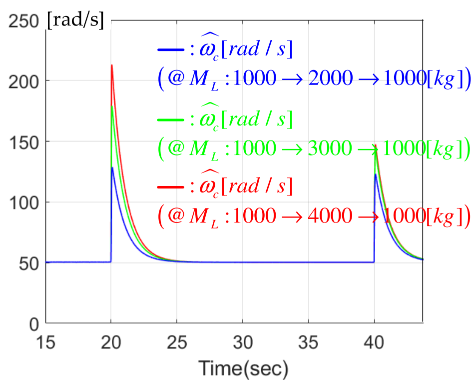

FIGURE 9. Current cutoff frequency responses under position regulation test for three load variation scenarios; M_L : 1000 → 2000/3000/4000 → 1000 *kg*.

TABLE 1. Numerical performance comparison result.

J	Tracking Mode			Regulation Mode			Avg.
	f_p =0.5Hz	f_p =2Hz	f_p =3Hz	$M_L[T]$: 1→2→1	M_L: 1→3→1	M_L: 1→4→1	
Proposed Controller	3712	2593	1251	2879	3121	3628	2864
Advanced Nonlinear Controller[28]	4628	2980	2118	4529	4827	7309	4399
BSC	5197	3751	2899	6511	7715	9412	5914

which collects the resultant data during the two operations in Sections V-A and V-B. This evaluation includes further comparisons of advanced proportional nonlinear controllers [28] including self-tuner to demonstrate the effectiveness of the proposed controller. Table. 1 shows the comparison result with the performance metric function J value. In summary, the comparison results show an average closed-loop performance improvement of 52 % for BSC and 35 % for advanced nonlinear controllers. This result implies that the proposed technique can be considered a reasonable alternative to conventional techniques because of its significant performance improvement in actual systems.

VI. CONCLUSION

This study incorporated a dynamic feedback loop mechanism into the control law to derive practical merits by increasing and decreasing the current-loop feedback gain according to the operating mode. Moreover, a plant parameter-information-free velocity observer was devised to enable the implementation of a pole-zero cancellation control action with active damping. The numerical simulation results confirmed the practical advantages of the proposed technique. However, there were numerous design parameters for the introduced auxiliary subsystems, which will be automatically determined through the offline optimization process developed in a future study. Furthermore, we will extend our study based on the neuro-adaptive control method combining neural networks to demonstrate robust performance against complex model uncertainties and nonlinearities.

REFERENCES

[1] Y. Jiang, Y. Deng, P. Zhu, M. Yang, and F. Zhou, "Optimization on size of Halbach array permanent magnets for magnetic levitation system for permanent magnet Maglev train," *IEEE Access*, vol. 9, pp. 44989–45000, 2021.

[2] Q. Ouyang, K. Fan, Y. Liu, and N. Li, "Adaptive LADRC parameter optimization in magnetic levitation," *IEEE Access*, vol. 9, pp. 36791–36801, 2021.

[3] Z. Wang, X. Li, Y. Xie, and Z. Long, "Maglev train signal processing architecture based on nonlinear discrete tracking differentiator," *Sensors*, vol. 18, no. 6, p. 1697, May 2018.

[4] J. Wang, L. Zhao, and L. Yu, "Adaptive terminal sliding mode control for magnetic levitation systems with enhanced disturbance compensation," *IEEE Trans. Ind. Electron.*, vol. 68, no. 1, pp. 756–766, Jan. 2021.

[5] J. Wang, L. Chen, and Q. Xu, "Disturbance estimation-based robust model predictive position tracking control for magnetic levitation system," *IEEE/ASME Trans. Mechatronics*, vol. 27, no. 1, pp. 81–92, Feb. 2021, doi: 10.1109/TMECH.2021.3058256.

[6] L. Zhang, S. A. Campbell, and L. Huang, "Nonlinear analysis of a Maglev system with time-delayed feedback control," *Phys. D, Nonlinear Phenomena*, vol. 240, no. 21, pp. 1761–1770, Oct. 2011.

[7] M. P. S. D. Santos, J. A. F. Ferreira, J. A. O. Simões, R. Pascoal, J. Torrão, X. Xue, and E. P. Furlani, "Magnetic levitation-based electromagnetic energy harvesting: A semi-analytical non-linear model for energy transduction," *Sci. Rep.*, vol. 6, no. 1, p. 18579, May 2016.

[8] Z. Zhang and L. Zhang, "Hopf bifurcation of time-delayed feedback control for Maglev system with flexible guideway," *Appl. Math. Comput.*, vol. 219, no. 11, pp. 6106–6112, Feb. 2013.

[9] H.-W. Lee, K.-C. Kim, and J. Lee, "Review of Maglev train technologies," *IEEE Trans. Magn.*, vol. 42, no. 7, pp. 1917–1925, Jul. 2006.

[10] J. S. Shamma and M. Athans, "Analysis of gain scheduled control for nonlinear plants," *IEEE Trans. Autom. Control*, vol. 35, no. 8, pp. 898–907, 2002.

[11] R.-J. Wai, J.-D. Lee, and K.-L. Chuang, "Real-time PID control strategy for Maglev transportation system via particle swarm optimization," *IEEE Trans. Ind. Electron.*, vol. 58, no. 2, pp. 629–646, Feb. 2011.

[12] C.-H. Kim, "Robust control of magnetic levitation systems considering disturbance force by LSM propulsion systems," *IEEE Trans. Magn.*, vol. 53, no. 11, pp. 1–5, Jul. 2017.

[13] Z. Zhang and X. Li, "Real-time adaptive control of a magnetic levitation system with a large range of load disturbance," *Sensors*, vol. 18, no. 5, p. 1512, May 2018.

[14] H. Ahmed, M. Ahsan, M. Benbouzid, A. Albarbar, M. Shahjalal, and S. Biricik, "Coordinate transformation-free observer-based adaptive estimation of distorted single-phase grid voltage signal," *IEEE Access*, vol. 8, pp. 74280–74290, 2020.

[15] R. M. Asl, R. Palm, H. Wu, and H. Handroos, "Fuzzy-based parameter optimization of adaptive unscented Kalman filter: Methodology and experimental validation," *IEEE Access*, vol. 8, pp. 54887–54904, 2020.

[16] Y. Chen, Z. Ming, and M. Menenti, "Change detection algorithm for multi-temporal remote sensing images based on adaptive parameter estimation," *IEEE Access*, vol. 8, pp. 106083–106096, 2020.

[17] M. Takizawa and M. Yukawa, "Joint learning of model parameters and coefficients for online nonlinear estimation," *IEEE Access*, vol. 9, pp. 24026–24040, 2021.

[18] R.-J. Wai and J.-D. Lee, "Robust levitation control for linear Maglev rail system using fuzzy neural network," *IEEE Trans. Control Syst. Technol.*, vol. 17, no. 1, pp. 4–14, Jan. 2009.

[19] Y. Sun, W. Li, J. Xu, H. Qiang, and C. Chen, "Nonlinear dynamic modeling and fuzzy sliding-mode controlling of electromagnetic levitation system of low-speed Maglev train," *J. Vibroeng.*, vol. 19, no. 1, pp. 328–342, Feb. 2017.

[20] R.-J. Wai and J.-D. Lee, "Backstepping-based levitation control design for linear magnetic levitation rail system," *IET Control Theory Appl.*, vol. 2, no. 1, pp. 72–86, Jan. 2008.

[21] U. Sadek, A. Sarjaš, A. Chowdhury, and R. Svečko, "Improved adaptive fuzzy backstepping control of a magnetic levitation system based on symbiotic organism search," *Appl. Soft Comput.*, vol. 56, pp. 19–33, Jul. 2017.

[22] J. Kaloust, C. Ham, J. Siehling, E. Jongekryg, and Q. Han, "Nonlinear robust control design for levitation and propulsion of a Maglev system," *IEE Proc.-Control Theory Appl.*, vol. 151, no. 4, pp. 460–464, Jul. 2004.

[23] S.-K. Kim and C. K. Ahn, "Velocity-sensorless proportional–derivative trajectory tracking control with active damping for quadcopters," *Nonlinear Dyn.*, vol. 103, no. 2, pp. 1681–1692, Jan. 2021.

[24] B. Sarsembayev, K. Suleimenov, and T. D. Do, "High order disturbance observer based PI-PI control system with tracking anti-windup technique for improvement of transient performance of PMSM," *IEEE Access*, vol. 9, pp. 66323–66334, 2021.

[25] V.-C. Nguyen, A.-T. Vo, and H.-J. Kang, "A finite-time fault-tolerant control using non-singular fast terminal sliding mode control and third-order sliding mode observer for robotic manipulators," *IEEE Access*, vol. 9, pp. 31225–31235, 2021.

[26] S.-K. Kim and C. K. Ahn, "Active damping injection controller for web longitude and tensions of nonlinear roll-to-roll systems," *Nonlinear Dyn.*, vol. 100, no. 4, pp. 3367–3379, Jun. 2020.

[27] J. Yang, A. Zolotas, W.-H. Chen, K. Michail, and S. Li, "Robust control of nonlinear MAGLEV suspension system with mismatched uncertainties via DOBC approach," *ISA Trans.*, vol. 50, no. 3, pp. 389–396, 2011.

[28] S.-K. Kim and C. K. Ahn, "Variable cut-off frequency algorithm-based nonlinear position controller for magnetic levitation system applications," *IEEE Syst. Man Cybern. Syst.*, vol. 1, pp. 1–7, 2019, doi: 10.1109/tsmc.2019.2945176.

[29] S.-K. Kim, "Nonlinear position stabilizing control with active damping injection technique for magnetic levitation systems," *Electronics*, vol. 8, no. 2, p. 221, Feb. 2019.

[30] S. Kim and C. K. Ahn, "Sensorless non-linear position-stabilising control for magnetic levitation systems," *IET Control Theory Appl.*, vol. 14, no. 17, pp. 2682–2687, Nov. 2020.

[31] V. K. Ingle and J. G. Proakis, *Essenstials of Digitals Signal Processing Using MATLAB*. Stamford, CT, USA: Cengage Learning, 2012.

[32] S.-K. Kim, K.-C. Kim, and C. K. Ahn, "Nonlinear signal-filtering technique with real-time gain booster for feedback system applications," *IEEE Signal Process. Lett.*, vol. 27, pp. 2183–2187, 2020.

[33] H. K. Khalil, *Nonlinear Systems*. Upper Saddle River, NJ, USA: Prentice-Hall, 2002.

SUNG HYUN YOU received the B.S. degree in electrical engineering from the Seoul National University of Science and Technology, Seoul, in 2013, and the Ph.D. degree from the School of Electrical Engineering, Korea University, Seoul, South Korea, in 2019. He is currently a Research Professor with the Research Institute of Engineering and Technology, Korea University. Since 2020, he has been an Assistant Professor at Chosun University, South Korea. His research interests include optimal, robust, intelligent, and receding horizon controls and estimations.

KI-CHAN KIM (Member, IEEE) was born in Busan, South Korea, in 1972. He received the bachelor's, master's, and Ph.D. degrees in electrical engineering from Hanyang University, Seoul, South Korea, in 1996, 1998, and 2008, respectively. From 1998 to 2005, he was a Chief Research Engineer with the Electro-Mechanical Research Institute, Hyundai Heavy Industries Company Ltd. Since 2005, he has been a Professor at the Department of Electrical Engineering, Hanbat National University, where he is also in-charge of the Center of Autonomous Car. His research interests include the design, analysis, experimentation, and control of driving systems, including motors, generators, inverters, and electromagnetic sensors for electric vehicles and railway trains. He is a member of the IEEE Industry Applications Society and a Board Member of KIEE. He received the Service Award at IEEE TEC'2019.

HYUN HO KANG received the B.S. degree in electrical engineering from Korea University, Seoul, South Korea, in 2017, where he is currently pursuing the Ph.D. degree with the School of Electrical Engineering. His research interests include optimal, robust, and intelligent control for unmanned aerial vehicles (UAVs) and multi-agent systems. He was a finalist at the Autonomous Drone Racing Competition of the IEEE International Conference on Fuzzy Systems, in 2021.

KWAN SOO KIM received the B.S. degree in electronic engineering from Kwnagwoon University, South Korea, in 2017. He is currently pursuing the Ph.D. degree with the Department of Electrical Engineering, Korea University, Seoul, South Korea. His research interests include optimal control, robust control, disturbance observer, finite impulse response filter, machine learning, neural networks, and nonlinear system control.

SEOK-KYOON KIM received the B.S. degree in electronic and IT media engineering from the Seoul National University of Science and Technology, Seoul, South Korea, in 2004, and the Ph.D. degree in electrical engineering from Korea University, Seoul, in 2014.

He worked at LG Electronics as a Senior Research Engineer, from 2015 to 2016, and he joined the Department of Creative Convergence Engineering, Hanbat National University, Daejeon, South Korea, in 2017. His research interests include the tracking problem of power electronic applications, such as power converters and motor drives, the power system stabilization problem, and the development of control theory, such as passivity-based control and nonlinear adaptive control.